Solar fuels photoanode materials discovery by integrating high-throughput theory and experiment

Qimin Yan[a,b,1,2], Jie Yu[c,d,e,2], Santosh K. Suram[c], Lan Zhou[c], Aniketa Shinde[c], Paul F. Newhouse[c], Wei Chen[d,3], Guo Li[a,b,e], Kristin A. Persson[d,f], John M. Gregoire[c,1], and Jeffrey B. Neaton[a,b,e,g,1]

[a]Molecular Foundry, Lawrence Berkeley National Laboratory, Berkeley, CA 94720; [b]Department of Physics, University of California, Berkeley, CA 94720; [c]Joint Center for Artificial Photosynthesis, California Institute of Technology, Pasadena, CA 91125; [d]Environmental Energy Technologies Division, Lawrence Berkeley National Laboratory, Berkeley, CA 94720; [e]Joint Center for Artificial Photosynthesis, Lawrence Berkeley National Laboratory, Berkeley, CA 94720; [f]Department of Materials Science and Engineering, University of California, Berkeley, CA 94720; and [g]Kavli Energy NanoSciences Institute at Berkeley, Berkeley, CA 94720

Edited by Thomas E. Mallouk, The Pennsylvania State University, University Park, PA, and approved February 6, 2017 (received for review December 4, 2016)

The limited number of known low-band-gap photoelectrocatalytic materials poses a significant challenge for the generation of chemical fuels from sunlight. Using high-throughput ab initio theory with experiments in an integrated workflow, we find eight ternary vanadate oxide photoanodes in the target band-gap range (1.2–2.8 eV). Detailed analysis of these vanadate compounds reveals the key role of VO_4 structural motifs and electronic band-edge character in efficient photoanodes, initiating a genome for such materials and paving the way for a broadly applicable high-throughput-discovery and materials-by-design feedback loop. Considerably expanding the number of known photoelectrocatalysts for water oxidation, our study establishes ternary metal vanadates as a prolific class of photoanode materials for generation of chemical fuels from sunlight and demonstrates our high-throughput theory–experiment pipeline as a prolific approach to materials discovery.

solar fuels materials | density-functional theory | high-throughput experiments | complex oxides | photocatalysis

The use of predictive simulation in combination with experiments for the accelerated discovery and rational design of functional materials is a challenge of significant contemporary interest. High-throughput computing and materials databases (1–3), largely based on density-functional theory (DFT), have recently enabled rapid screening of solid-state compounds with simulation for multiple properties and functionalities (4–10). Since their advent just a few years ago, these DFT-based databases and analytics tools have already been used to identify more than 20 new functional materials that were later confirmed by experiments across a number of applications (8), motivating concerted efforts to validate theory predictions with experiments (11). However, in photoelectrochemistry for the renewable synthesis of solar fuels, efficient metal-oxide photoanode materials—photoelectrocatalysts for the oxygen evolution reaction (OER)—remain critically missing (12). Forty years of experimental research has yielded just 16 metal-oxide photoanode compounds with band-gap energy in the desirable 1.2–2.8-eV range that strongly overlaps with the solar spectrum. Prior high-throughput computational screening studies have yet to expand this list (6, 7, 13), in part due to quantitative limitations in predictability of the electronic structure—especially band-gap energy, E_g, and the valence band maximum (VBM) energy, E_{VBM}—from the chemical composition and crystal structure. Our integration of ab initio theory with high-throughput experiments has yielded a most prolific materials discovery effort, as demonstrated by the identification of 12 water oxidation photoelectrocatalysts in the target band-gap range, including our recently reported 4 copper vanadates (14) and 8 additional metal vanadates reported here.

Monoclinic $BiVO_4$ (15) has received substantial attention as a solar fuels photoanode material due to its promising OER photoactivity. It has a desirable 2.4-eV band gap derived from a conduction band minimum (CBM) consisting of V 3d states, and a VBM of mixed O 2p and Bi 6s character (16). We recently identified another ternary vanadate, β-$Mn_2V_2O_7$, that, although not photoactive for the OER, exhibits a 1.8-eV band gap and valence band alignment to the OER equilibrium energy, or OER potential, a result of hybridization of Mn 3d with O 2p states. β-$Mn_2V_2O_7$ shares a common VO_4 structural motif with $BiVO_4$: Both compounds possess $3d^0$ V cations tetrahedrally coordinated by oxygen. Orbital hybridization resulting from this VO_4 motif engenders significant baseline O 2p and V 3d character at the VBM and CBM, creating an electronic structure "scaffold" that enables the formation of a desirable E_g and E_{VBM} upon introduction of an additional metal cation (17). For example, in $BiVO_4$ and β-$Mn_2V_2O_7$, additional hybridization of O 2p with Mn 3d and Bi 6s states, respectively, leads to an increase in the E_{VBM} toward the OER potential. Here, we hypothesize that this VO_4-scaffold phenomenon applies broadly to ternary vanadates. Indeed, we observe that three additional previously known OER photoanodes with band-gap energies between 1.2 and 2.8 eV [α-Ag_3VO_4 (18), $FeVO_4$ (19, 20), and β-$Cu_3V_2O_8$ (21)] are also ternary vanadates with a VO_4 structural motif in the $3d^0$ electronic configuration. For these reasons, VO_4-based ternary compounds are fertile ground for both discovering metal-oxide photoanodes and seeding the photoanode materials genome.

Current computational and experimental approaches differ in the material properties they can most efficiently and effectively characterize, and by leveraging their complementarity we can both accelerate the materials discovery process and confirm the validity of each approach. After several generations of integrated computational and experimental materials screening workflows, we arrived at the tiered screening pipeline of Fig. 1 in which we (*i*) selectively mine a materials database with a well-defined hypothesis to arrive at a subset of promising materials; (*ii*) screen

Significance

Combining high-throughput computation and experiment accelerates the discovery of photoelectrocatalysts for water oxidation and explains the origin of their functionality, establishing ternary metal vanadates as a prolific class of photoanode materials for generation of chemical fuels from sunlight.

Author contributions: Q.Y., K.A.P., J.M.G., and J.B.N. designed research; Q.Y., J.Y., S.K.S., L.Z., A.S., P.F.N., W.C., and G.L. performed calculations and experiments; Q.Y., S.K.S., K.A.P., J.M.G., and J.B.N. analyzed data; and Q.Y., J.M.G., and J.B.N. wrote the paper with contributions from all authors.

The authors declare no conflict of interest.

This article is a PNAS Direct Submission.

[1]To whom correspondence may be addressed. Email: qiminyan@temple.edu, gregoire@caltech.edu, or jbneaton@berkeley.edu.

[2]Present address: Department of Physics, Temple University, Philadelphia, PA 19122.

[3]Present address: Department of Mechanical, Materials, and Aerospace Engineering, Illinois Institute of Technology, Chicago, IL 60616.

This article contains supporting information online at www.pnas.org/lookup/suppl/doi:10.1073/pnas.1619940114/-/DCSupplemental.

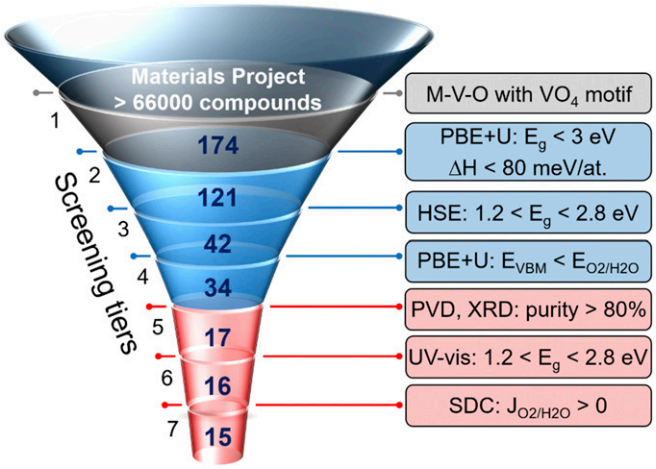

Fig. 1. Tiered screening pipeline for accelerated discovery of solar fuels photoanodes. The number of compounds (bold) and screening criteria used in this study for the seven-tier pipeline that integrates database mining (gray), high-throughput computational screening (blue), and high-throughput experimental screening (red).

this materials subset for select properties with high-throughput computation at appropriate levels of theory; and (*iii*) use companion combinatorial experiments on the same subset to both validate the calculations and characterize material performance under device-relevant conditions. In the present work we demonstrate the efficacy of this approach for the discovery of ternary vanadate photoanodes and note that the strategies outlined herein are broadly applicable for discovery of functional materials.

To evaluate the VO_4-scaffold hypothesis, the 7 tiers of screening commence with a query of the Materials Project (MP) database (1) to identify 174 known VO_4-based ternary vanadates. Out of these 174 ternary vanadate compounds, 147 compounds are indexed in the Inorganic Crystal Structure Database as previously synthesized materials, and the remaining 27 compounds are the results of previous structure prediction calculations within the MP. For each compound, the database also provides the DFT formation energy above the convex hull in the composition phase diagram (ΔH) and a coarse estimate of E_g. These quantities are computed using DFT with the generalized gradient approximation of Perdew, Burke, and Ernzerhof (PBE) and Hubbard U (22) corrections for metal cation d states with the Vienna Ab initio Simulation Package (VASP) code (23). Our DFT-PBE+U calculations provide a high-throughput tier 2 screen that thresholds ΔH and E_g in an effort to avoid nonsynthesizable materials (6) and known wide-gap insulators, respectively. To more accurately screen and identify semiconductors with E_g in the target range, we note that a higher level of theory would be in principle required, such as ab initio many-body perturbation theory (24), at significantly greater computational expense. As a compromise that balances computational efficiency with adequate accuracy, we proceed in practice with DFT but use generalized Kohn–Sham states obtained from the hybrid functional of Heyd, Scuseria, and Ernzerhof (HSE) with a modified mixing parameter, α, of 0.17 (*SI Appendix*) that results in more tolerant acceptance criteria for tier 3. The HSE functional features improved treatment of short-range exchange and correlation effects relative to PBE+U that treat delocalized sp valent and localized d states on equal footing (25) and can lead to more predictive band gaps (26). Finally, in tier 4, we evaluate E_{VBM} using a combination of bulk HSE (α = 0.17) and surface slab PBE+U calculations (27, 28) to determine if the VBM meets the OER thermodynamic requirement (*SI Appendix*). Surface dipoles that arise upon interfacing the metal oxides with water are expected to slightly raise E_{VBM} (28); evaluating E_{VBM} relative to vacuum, as we do here, is therefore a particularly lenient screening criterion for allowing the ensuing experiments to demonstrate operational VBM alignment via photocurrent measurements.

To validate these screening criteria and their propensity for identifying photoanode materials, we turn to combinatorial experiments. The most common bottleneck in computation-guided experimental work is synthesis of the target materials in a device-relevant format, prompting our development of combinatorial sputtering and annealing methods in which thin-film synthesis is attempted for each target phase (and its off-stoichiometry variants) using a variety of reactive sputtering and annealing conditions. The materials exhibiting target-phase purity in excess of 80% pass to tiers 6 and 7, where high-throughput optical spectroscopy (UV-vis) and photoelectrochemistry characterize E_g (direct and indirect transitions) and the photocurrent density at the Nernstian potential ($J_{O2/H2O}$), respectively. It is important to note that for these final tiers of screening, the optical and photoelectrochemical properties are measured not only for the target phase but also neighboring phases in the composition space, enabling identification of E_g and $J_{O2/H2O}$ values that are representative of the target phase. The high-throughput $J_{O2/H2O}$ measurements use sufficiently energetic photons (~3.2 eV) to excite semiconductors across the entire E_g range.

The list of tier 4 compounds is provided in *SI Appendix* and includes several examples of multiple polytypes with a common formula unit, and often a subset of these polytypes are synthesized in high purity using the combinatorial synthesis techniques. Other phases may not be accessible with these synthesis techniques due to kinetic limitations or the presence of stable phases that are absent from the MP database. In total, 17 high-purity compounds were obtained, comprising tier 5 of the screening

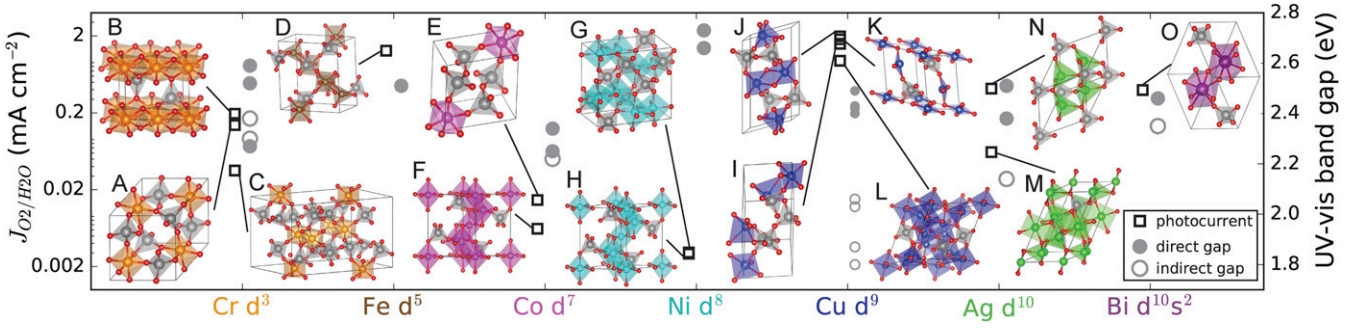

Fig. 2. Landscape of photoactive structures identified by the pipeline. The experimentally measured band-gap energy and OER photocurrent density are shown for 15 ternary vanadate photoanodes (*A–O*; see Table 1) organized by cation electronic configuration. The respective crystal structures share a common VO_4 motif (gray tetrahedra with gray V and red O) and span a broad range of structures (colored by cation element).

Table 1. The 15 phases identified by the screening pipeline are listed with the corresponding direct (DA) and indirect (IA) band gap values from tier 3 and tier 6 of the pipeline

Fig. 2 label	Phase	DFT-HSE band gap, eV		UV-vis band gap, eV		$J_{O2/H2O}$, mA cm^{-2}	Refs.
		DA	IA	DA	IA		
A	$Cr_2V_4O_{13}$	2.56	2.55	2.52	2.30	0.139	
B	orth-$CrVO_4$	2.38	2.21	2.59	2.38	0.20	
C	mon-$CrVO_4$	2.48	2.48	2.27	<2.27	0.036	
D	tri-$FeVO_4$	2.14	2.10	2.51	<2.3	1.3	19 20
E	α-CoV_2O_6	2.17	2.16	2.25	<2.25	0.015	
F	$Co_3V_2O_8$	2.06	2.03	2.34	2.22	0.006	
G	$Ni_2V_2O_7$	2.75	2.72	2.73	<2.5	0.003	
H	$Ni_3V_2O_8$	2.55	2.54	2.66	<2.5	0.003	
I	α-$Cu_2V_2O_7$	1.98	1.84	2.43	2.06	1.6	32
J	β-$Cu_2V_2O_7$	1.84	1.84	2.42	2.03	2.0	32
K	γ-$Cu_3V_2O_8$	1.89	1.73	2.40	1.80	1.8	32
L	$Cu_{11}V_6O_{26}$	1.41	1.38	2.49	1.87	0.95	32
M	α-Ag_3VO_4	2.07	1.70	2.38	2.14	0.062	18
N	β-Ag_3VO_4	1.91	1.61	2.51	<2.51	0.41	
O	mon-$BiVO_4$	2.83	2.72	2.46	2.35	0.396	15

The photocurrent density from tier 7 is also provided along with references for the copper vanadates identified by the pipeline of Fig. 1 (32) and the three previously reported, experimentally discovered OER photoanodes.

pipeline. Band-gap estimation through automated Tauc analysis experimentally verified the band-gap energy range for 16 of these 17 phases, demonstrating the fidelity of our DFT-HSE (α = 0.17) band-gap calculations. The most striking acceptance rate in the screening pipeline is the final screening criterion, where 15 of 16 phases exhibited photoactivity when biased at the OER potential, an exceptionally high hit rate of 94%.

The 15 metal-oxide photoanodes identified by the pipeline are illustrated in Fig. 2, demonstrating that desirable E_g and photoactivity are obtained for ternary vanadates with a range of cation elements and respective electronic configurations, a marked departure from the d^0 configuration of photoanodes such as TiO_2 and WO_3. The band-gap and $J_{O2/H2O}$ values are also listed in Table 1, which includes three photoanodes reported by other investigators, validating the pipeline's ability to replicate known results. Several other phases in Table 1 have been explored as photoactive materials for different reactions or conditions [γ-$Cu_3V_2O_8$ (29), $Cr_2V_4O_{13}$ (30), and β-Ag_3VO_4 (14) for photodegradation of organics and $Ni_3V_2O_8$ as a powder photocatalyst for water oxidation (31)] but have not been studied or demonstrated as photoanodes. The materials identified by the screening pipeline greatly expand the compendium of known photoanodes with band-gap energy in the 1.2–2.8-eV range and demonstrate the efficacy of integrating high-throughput computational and experimental screening.

We can further evaluate the VO_4-scaffold hypothesis by quantifying the chemical character of the valence and conduction bands (with respect to the O 2p – V 3d scaffold) for the 91 ternary vanadates from tier 2 that possess a V $3d^0$ electronic configuration. The results, shown in Fig. 3, confirm our hypothesis, demonstrating that E_g can be tuned over a broad 3-eV range through tailoring the VO_4 band-edge character via orbitals from an additional cation element and crystal structure. Band-gap tuning into the desirable range can be attained via moderate hybridization at either or both of the conduction and valence bands edges, and photoelectrochemical activity is obtained over a diverse set of band-character parameters and band-gap energies. We note that hybridization that enables the tuning of E_{VBM} is particularly critical for optimizing photoanode efficiency.

The results of this discovery pipeline, particularly when combined with existing literature, identify ternary vanadates as a remarkable class of photoanode materials. Out of the 28 known photoanodes from present and previous work, 22 contain V with 16 of those exhibiting the pure VO_4 motif. Fig. 3 identifies the band-character parameters as important descriptors for understanding and designing improved materials in this class. Additional characterization of the Cu-based phases discovered by this pipeline has been reported by us (32) and others (33), and we note that the collection of discoveries motivates additional studies, including (*i*) the exploitation of band-edge tuning to optimize energetics, (*ii*) the characterization of photoactivity over the full solar spectrum, and (*iii*) the engineering of electrochemical stability through choice of operating pH and protective or self-passivating layers, all of which are enabled by the range of vanadate chemistries identified by the pipeline. The characterization and optimization of stability is paramount to establishing a deployable photoanode, an area requiring concerted future theory and experimental effort, particularly due to the recently demonstrated propensity for ternary oxides to self-passivate under operational conditions (34).

For solar hydrogen generation with a tandem light absorber, device models (35) indicate that lowering the photoanode band gap from the $BiVO_4$ gap of 2.4 eV to the 1.8-eV value observed with several tier-7 compounds can elicit a 2- to 3-fold enhancement in device efficiency, highlighting the opportunities provided by our discovery of low-band-gap photoanodes. As with well-established photoanodes such as $BiVO_4$ and Fe_2O_3, each photoanode reported here will require extensive research and development to optimize its solar energy conversion efficiency. This successful

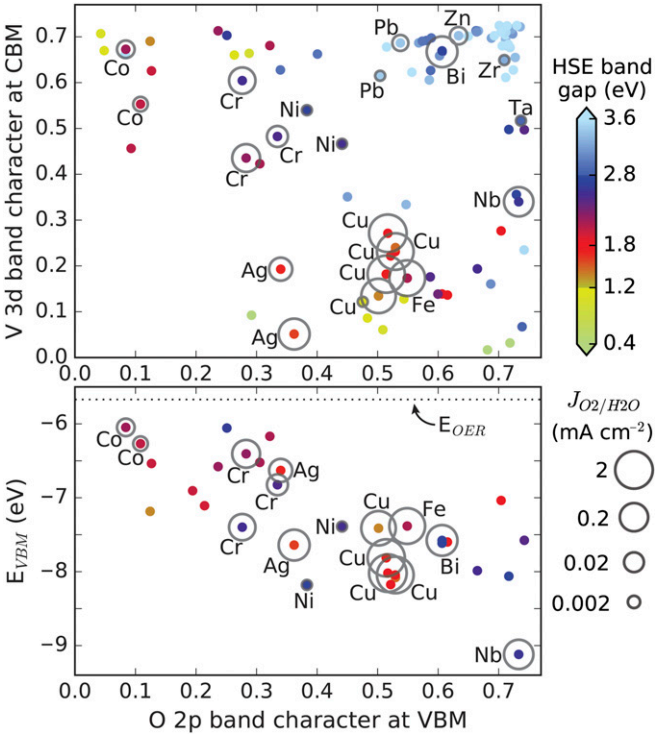

Fig. 3. Tuning band gap and band alignment with hybridization. The orbital character at the band edges [*Top*; band-character scale is 0–1 and determined from HSE (α = 0.17) calculations] for 91 VO_4-based ternary vanadates is shown with false-color representation of the HSE (α = 0.17) band-gap energy. Experimentally verified photoanodes are circled according to the photocurrent density measured after 44 s of illumination toggling (385 nm) in pH 9 electrolyte (labels indicate the cation element). The efficacy of valence band hybridization in improving VBM alignment to the OER equilibrium energy is demonstrated for 30 of these vanadates (*Bottom*).

implementation of high-throughput materials discovery, where complementary computational and experimental techniques are carefully integrated, introduces a paradigm of materials research in which hypothesis-driven studies can be conducted with significantly improved efficiency.

ACKNOWLEDGMENTS. The authors thank Anubhav Jain and Joel Haber for helpful discussions. Computational work was supported by the Materials Project Predictive Modeling Center through the US Department of Energy (DOE), Office of Basic Energy Sciences, Materials Sciences and Engineering Division, under Contract DE-AC02–05CH11231. Experimental work was performed by the Joint Center for Artificial Photosynthesis, a DOE Energy Innovation Hub, supported through the Office of Science of the US DOE (Award DE-SC0004993). Work at the Molecular Foundry was supported by the Office of Science, Office of Basic Energy Sciences, of the US DOE under Contract DE-AC02–05CH11231. Computational resources were also provided by the DOE through the National Energy Supercomputing Center, a DOE Office of Science User Facility supported by the Office of Science of the US DOE under Contract DE-AC02-05CH11231.

1. Jain A, et al. (2013) Commentary: The Materials Project: A materials genome approach to accelerating materials innovation. *APL Mater* 1(1):011002.
2. Saal JE, Kirklin S, Aykol M, Meredig B, Wolverton C (2013) Materials design and discovery with high-throughput density functional theory: The Open Quantum Materials Database (OQMD). *JOM* 65(11):1501–1509.
3. Curtarolo S, et al. (2012) AFLOWLIB.ORG: A distributed materials properties repository from high-throughput ab initio calculations. *Comput Mater Sci* 58:227–235.
4. Curtarolo S, et al. (2013) The high-throughput highway to computational materials design. *Nat Mater* 12(3):191–201.
5. Hautier G, Miglio A, Ceder G, Rignanese GM, Gonze X (2013) Identification and design principles of low hole effective mass p-type transparent conducting oxides. *Nat Commun* 4:2292.
6. Wu YB, Lazic P, Hautier G, Persson K, Ceder G (2013) First principles high throughput screening of oxynitrides for water-splitting photocatalysts. *Energy Environ Sci* 6(1): 157–168.
7. Castelli IE, et al. (2012) Computational screening of perovskite metal oxides for optimal solar light capture. *Energy Environ Sci* 5(2):5814–5819.
8. Jain A, Shin Y, Persson KA (2016) Computational predictions of energy materials using density functional theory. *Nat Rev Mater* 1:15004.
9. Sendek AD, et al. (2017) Holistic computational structure screening of more than 12 000 candidates for solid lithium-ion conductor materials. *Energy Environ Sci* 10(1): 306–320.
10. Gautier R, et al. (2015) Prediction and accelerated laboratory discovery of previously unknown 18-electron ABX compounds. *Nat Chem* 7:308–316.
11. Perim E, et al. (2016) Spectral descriptors for bulk metallic glasses based on the thermodynamics of competing crystalline phases. *Nat Commun* 7:12315.
12. Woodhouse M, Parkinson BA (2008) Combinatorial discovery and optimization of a complex oxide with water photoelectrolysis activity. *Chem Mater* 20(7):2495–2502.
13. Castelli IE, et al. (2012) New cubic perovskites for one- and two-photon water splitting using the computational materials repository. *Energy Environ Sci* 5(10):9034–9043.
14. Xu J, et al. (2012) Synthesis and visible light photocatalytic activity of β-AgVO3 nanowires. *Solid State Sci* 14(4):535–539.
15. Sayama K, et al. (2003) Photoelectrochemical decomposition of water on nanocrystalline BiVO4 film electrodes under visible light. *Chem Commun (Camb)* 23(23): 2908–2909.
16. Walsh A, Yan Y, Huda MN, Al-Jassim MM, Wei SH (2009) Band edge electronic structure of BiVO4: Elucidating the role of the Bi s and V d orbitals. *Chem Mater* 21: 547–551.
17. Yan Q, et al. (2015) Mn2V2O7: An earth abundant light absorber for solar water splitting. *Adv Energy Mater* 5(8):1401840.
18. Chemelewski WD, Mabayoje O, Mullins CB (2015) SILAR growth of Ag3VO4 and characterization for photoelectrochemical water oxidation. *J Phys Chem C* 119(48): 26803–26808.
19. Mandal H, et al. (2016) Development of ternary iron vanadium oxide semiconductors for applications in photoelectrochemical water oxidation. *RSC Advances* 6(6): 4992–4999.
20. Morton CD, Slipper IJ, Thomas MJK, Alexander BD (2010) Synthesis and characterisation of Fe–V–O thin film photoanodes. *J Photochem Photobiol Chem* 216(2–3): 209–214.
21. Seabold JA, Neale NR (2015) All 1st row transition metal oxide photoanode for water splitting based on $Cu_3V_2O_8$. *Chem Mater* 27(3):1005–1013.
22. Anisimov V, Aryasetiawan F, Lichtenstein AI (1997) First-principles calculations of the electronic structure and spectra of strongly correlated systems: The LDA+U method. *J Phys Condens Matter* 9(4):767–808.
23. Kresse G, Furthmuller J (1996) Efficiency of ab-initio total energy calculations for metals and semiconductors using a plane-wave basis set. *Comput Mater Sci* 6(1): 15–50.
24. Onida G, Reining L, Rubio A (2002) Electronic excitations: Density-functional versus many-body Green's-function approaches. *Rev Mod Phys* 74(2):601–659.
25. Heyd J, Scuseria GE, Ernzerhof M (2006) Hybrid functionals based on a screened Coulomb potential. *J Chem Phys* 124(21):219906.
26. Heyd J, Peralta JE, Scuseria GE, Martin RL (2005) Energy band gaps and lattice parameters evaluated with the Heyd-Scuseria-Ernzerhof screened hybrid functional. *J Chem Phys* 123(17):174101.
27. Moses PG, Miao M, Yan Q, Van de Walle CG (2011) Hybrid functional investigations of band gaps and band alignments for AlN, GaN, InN, and InGaN. *J Chem Phys* 134(8): 084703.
28. Stevanović V, Lany S, Ginley DS, Tumas W, Zunger A (2014) Assessing capability of semiconductors to split water using ionization potentials and electron affinities only. *Phys Chem Chem Phys* 16(8):3706–3714.
29. Min W, Liu Q (2011) Synthesis and photocatalytic property of $Cu_3V_2O_8$ prepared by liquid phase precipitation. *Adv Mat Res* 236-238:1675–1678.
30. Kalal S, Pandey A, Ameta R, Punjabi PB (2016) Heterogeneous photo-Fenton-like catalysts Cu2V2O7 and Cr2V4O13 for an efficient removal of azo dye in water. *Cogent Chem* 2(1):1143344.
31. Wang D, Tang J, Zou Z, Ye J (2005) Photophysical and photocatalytic properties of a new series of visible-light-driven photocatalysts M3V2O8 (M = Mg, Ni, Zn). *Chem Mater* 17(20):5177–5182.
32. Zhou L, et al. (2015) High throughput discovery of solar fuels photoanodes in the CuO-V2O5 system. *Adv Energy Mater* 5(22):1500968.
33. Guo WL, et al. (2015) Synthesis and characterization of CuV2O6 and Cu2V2O7: Two photoanode candidates for photoelectrochemical water oxidation. *J Phys Chem C* 119(49):27220–27227.
34. Zhou L, et al. (2016) Stability and self-passivation of copper vanadate photoanodes under chemical, electrochemical, and photoelectrochemical operation. *Phys Chem Chem Phys* 18(14):9349–9352.
35. Fountaine KT, Lewerenz HJ, Atwater HA (2016) Efficiency limits for photoelectrochemical water-splitting. *Nat Commun* 7:13706.